Falling Film Measurements using High Speed Camera and High Speed Infra-Red Camera

Thilagan Kannappan[1] and Mani Annamalai[1]

[1]Department of Mechanical Engineering

Indian Institute of Technology Madras, Chennai, Tamil Nadu, 600036 (India)

Abstract

In this paper, a non-intrusive technique was developed to measure falling film thickness and temperature simultaneously based on the image processing techniques. This non-intrusive technique is used to study the heat and mass transfer characteristics. The enhanced heat and mass transfer of falling film over the tube will be used in the desalination system for distillate water production. The A high speed camera and a high speed infra-red camera are used to record falling film formation and temperature respectively over a horizontal plain tube at the rate of 10,000 fps by simultaneous triggering. The recorded images are processed using image processing software packages to determine film thickness and temperature profile at different circumferential angles ranging from 0^o to 180^o with tube impingement height of 5 mm. Film thickness over the horizontal plain tube is taken at different flow rates in the range of 0.6 lpm to 2 lpm. Measured film temperatures and film thicknesses are compared with the literature data. It is observed that the error band for falling film thickness is in the range of ±3.20% to ±8.29% for different falling film Reynolds numbers. Also, the error band for falling film temperature is in the range of ±0.08% to ±1.57%, when compared with calibrated thermocouples.

Keywords: Film thickness, Film temperature, Horizontal plain tube, Image processing

1. Introduction

A falling film is a common and effective mode of heat transfer application in many industries, such as desalination for potable drinking water, refrigeration for cooling and cold storage, Ocean thermal energy conversion (OTEC) for power generation, dairy farms and so on. The most common and widely used type of heat transfer is in multi-effect desalination (MED) application for producing fresh water on a large commercial scale (Al-Shammiri and Safar, 1999; Khawaji et al., 2008; Nair and Kumar, 2013; Ophir and Lokiec, 2005). In order to enhance the effective heat transfer using the falling film method, a proper and accurate measuring technique needs to be developed to measure thin film thickness over the horizontal tubes in the evaporation of the MED system (Chen et al., 2015; Xu et al., 2004).

Researchers have developed numerical models to determine film thickness at different circumferential angles. In 1916, Nusselt numerically modelled film thickness measurement by considering thermophysical properties, fluid flow rate and acceleration due to gravity (Nusselt, 1916). Later, researchers found that there was a lacuna in Nusselt's numerical model to determine film thickness. In 2012, Hou et al. found that the diameter of the pipe and impingement height between pipes will play a major role in determining the film thickness. So, authors modified the Nusselt's equation by giving the ratio of impingement height between pipes and diameter of the pipe with constant values based on their experimental trials (Hou et al., 2012; Nusselt, 1916).

Many researchers have attempted to measure film thickness by intrusive and non–intrusive methods. In intrusive methods, Hou et al. 2012, measured the film thickness using displacement micrometer measurement with the tube impingement height ranging from 10 mm to 40 mm with Reynolds numbers ranging from 150 to 800. The working fluids used for their experiment were pure water and seawater. They observed that Nusselt's numerical model gave a relatively reasonable prediction of the film thickness around the upper perimeter of the tube; but a poor prediction around the lower perimeter (Hou et al., 2012). Zhang et al. 2020, measured falling film thickness over a horizontal corrugated tube using a displacement micrometer. They used pure water, maintained at 20^{o}C, as working fluid with Reynolds numbers ranging from 150 to 1000 and observed that the film thickness of the corrugated tube

doi:10.18086/eurosun.2022.09.02 Available at http://proceedings.ises.org

increases with the increase of the film Reynolds number, which is the thinnest for circumferential angle ranging from 90^o to 120^o. The film thickness decreases by increasing the tube spacing, increasing the tube diameter and corrugation radius (Zhang et al., 2020).

Researchers have started developing non-intrusive methods to evaluate the characters of the liquid film. In 2019, Jayakumar et al. have measured the falling film thickness using an air-coupled ultrasonic transducer for plain horizontal tube. They used drinking water, maintained at 25^{o}C, as the working fluid for different Reynolds numbers ranging from 130 to 350. They measured the film thickness for the circumferential angle ranging from 40^o to 130^o. They observed fluctuation in film thickness with increase in flow rate and this technique can also process film thickness data with better accuracy in minimal time (Jayakumar et al., 2019). Later in 2021, Maliackal et al. measured the falling film thickness using a laser interferometric technique. They used drinking water, which was maintained in the range from 70^{o}C to 90^{o}C, as the working fluid for different Reynolds numbers ranging from 350 to 900. They used an optical shadow graph technique to evaluate the falling film thickness around the circumference of a horizontal tube. Mach Zehnder Interferometer (MZI) was utilized to visualize the isotherm formation. The film thickness was measured at the circumferential angles ranging from 10^o to 170^o and observed that the film thickness variation around the tube circumference shows an increasing trend with increase in Reynolds number, but a change in trend with varying feed inlet temperatures (Maliackal et al., 2021). In 2022, Maliackal et al. were able to measure the film interface temperature (Maliackal et al., 2022a, 2022b). The characteristics of falling film of a horizontal tube is purely depend on liquid film temperature and thickness. Based on the work carried out by the researchers using non-intrusive techniques, a simultaneous measurement is developed for the different film characteristics.

This work presents a novel image processing technique for simultaneous measurements of falling film thickness and temperature of a horizontal plain tube of a falling film evaporator of a Multi-Effect Evaporator of desalination system.

2. Principle of operation

Experimental setup consists of a uniform water distributor tank, measuring tube and dummy tubes in a horizontal arrangement, constant temperature water bath, ultrasonic type flow meter and recirculation pump. The uniform water distributor tank is of dimension 60 mm x 50 mm x 150 mm (height x width x length). A baffle is provided at the height of 40 mm from the bottom of the uniform water distributor tank. A slot opening of 1 mm at the top of the uniform water distributor tank is provided for uniform sheet flow to simulate the flow conditions of the evaporator in the desalination plant.

The working fluid for the experiment is taken as drinking water. The water temperature is maintained using a constant temperature water bath. Water is pumped to the uniform water distributor tank from the constant temperature bath. Water flows through the distributor tank's slot and flows over the first three consecutive dummy tubes, measurement tube (fourth tube) and dummy tube (fifth tube) as shown in Fig. 1. The first three dummy tubes are used for flow stabilization and for uniform film formation over the measurement tube. The fifth dummy tube is used to avoid splashing of water before it collects in the water collection tank. The tube dimension, spacing and other characteristics are given in Table 1. At the bottom, water gets collected in the collection tank and flows back to the constant temperature water bath tank. The operating conditions for the experimental study are given in Table 2. The flow rate and working fluid temperatures before and after the measurement tube are continuously monitored using a calibrated ultrasonic flow meter and T - type thermocouples respectively. T - type thermocouples are inserted through the body of the experimental setup and touches the water without disturbing the film formation. Figure 2 shows the photographic view of falling film experimental setup.

Tab. 1: Tube characteristic.

Tube material	Copper
Tube Diameter (ID)	25.4 mm
Tube thickness	0.2 mm
Effective tube length	150 mm
Number of dummy tubes	4
Number of dummy catch tube	1

Ambient Temperature	28ºC

Tab. 2: Experimental operating conditions.

Working fluid	Drinking water
Operating working fluid flow rate	0.6 – 2 lpm
Operating working fluid temperature	60 ºC

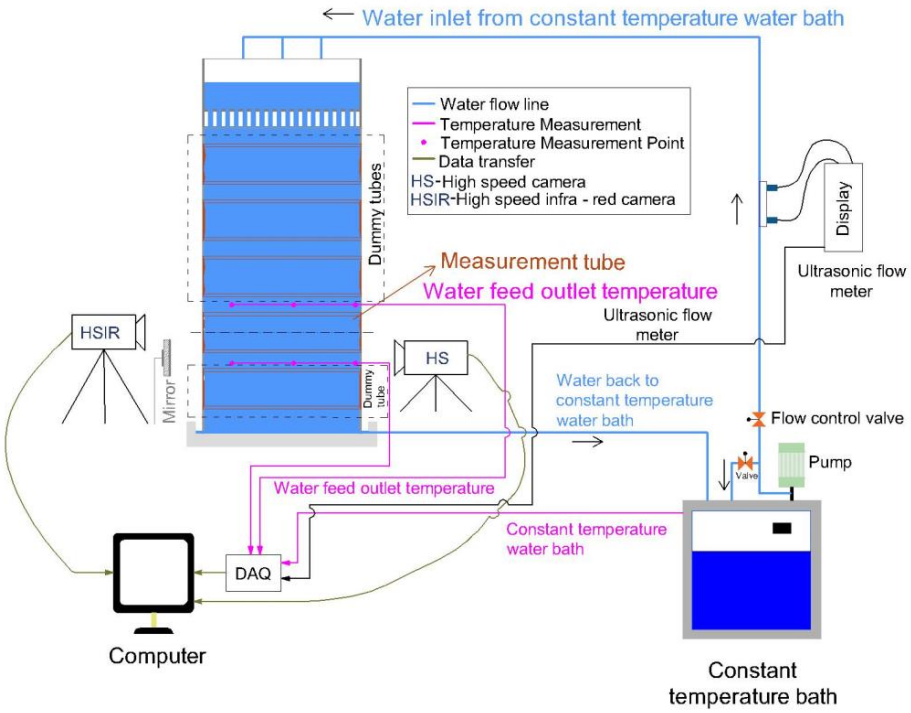

Fig. 1: Schematic diagram of falling film experimental setup.

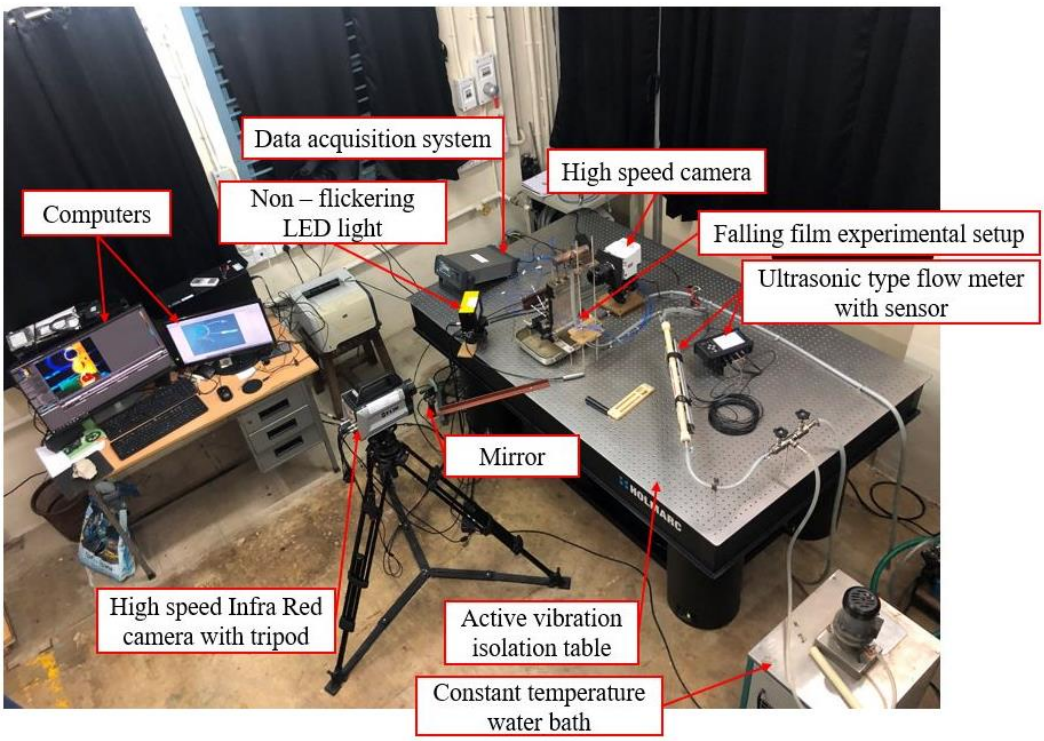

Fig. 2: Photograph of falling film experimental setup.

3. Falling film thickness and temperature measurement

Figure 3 shows the flow process for the mean film thickness and temperature measurements at each 10° circumferential angle of plain horizontal tube. After stabilization of film formation over the measuring horizontal tube, non – flickering light is positioned. The position of non-flickering light is kept in such a way that reflection of light from mirror, falling film and other surfaces should be minimal. Phantom VEO 1310L high-speed camera is made to focus the film formation from the mirror with surface finish of λ/10 and FLIR X6901sc high-speed infra-red camera is made to focus the film falling over the horizontal tube. After aligning non-flickering light, high-speed camera and high-speed infra-red camera, trial shots are recorded to check the focus and aligning. On completion of this process, high-speed camera and high-speed infra-red camera are triggered simultaneously to capture the film formation and temperature of falling film over the horizontal tube respectively.

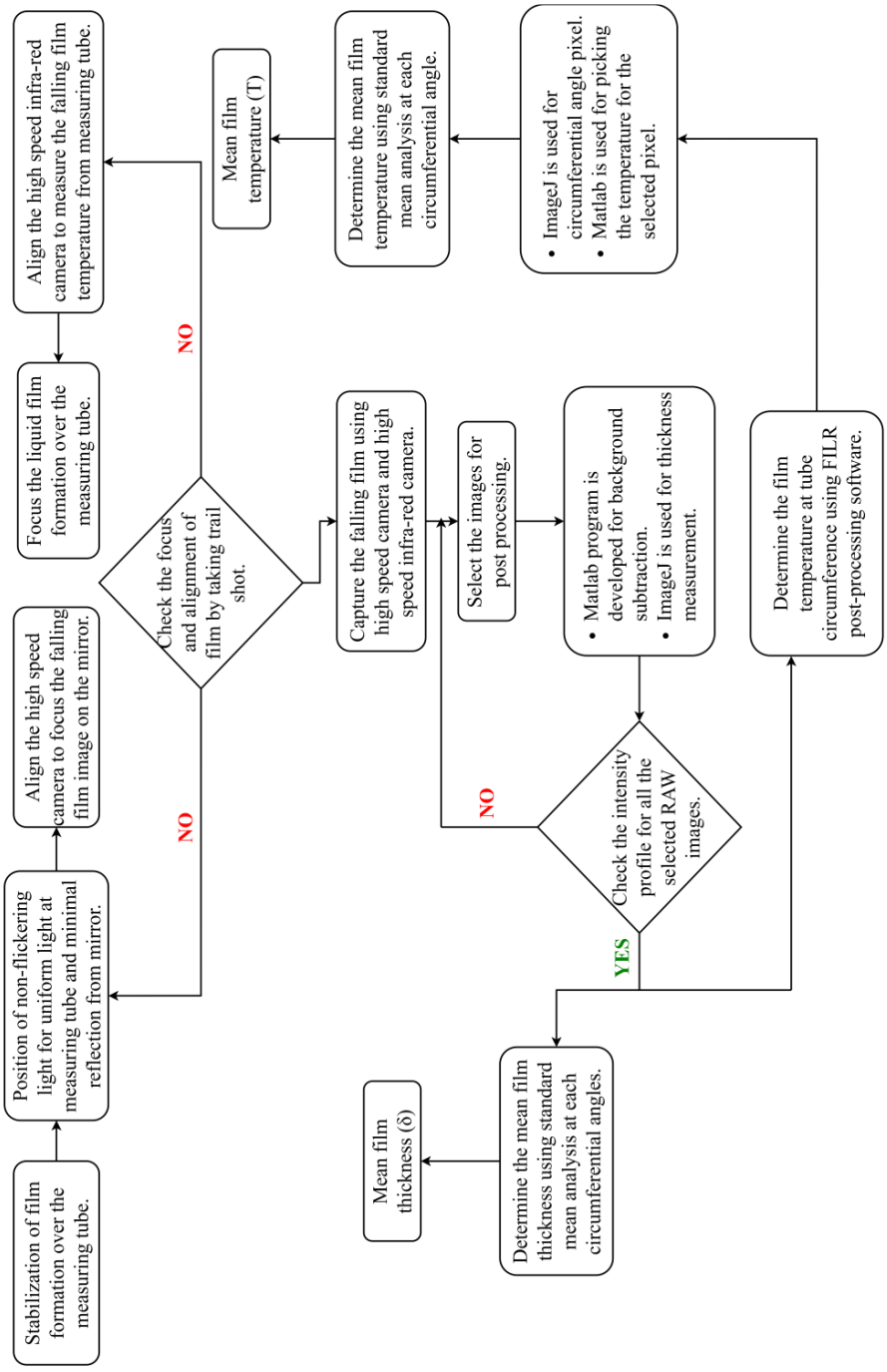

Fig. 3: Process flow chart for film thickness and temperature measurements.

After simultaneous capturing, random images of high speed camera are selected for post processing. An in house MATLAB program is developed to remove unwanted noises like reflection of light and to identify liquid film flow. Figures 4a and 4b show the raw images of high speed camera without flow and with flow respectively before post processing. Figures 5a and 5b show the images of high speed camera without flow and with flow respectively after post processing for the flow rate of 1 lpm corresponding to Reynolds number of 1008.94.

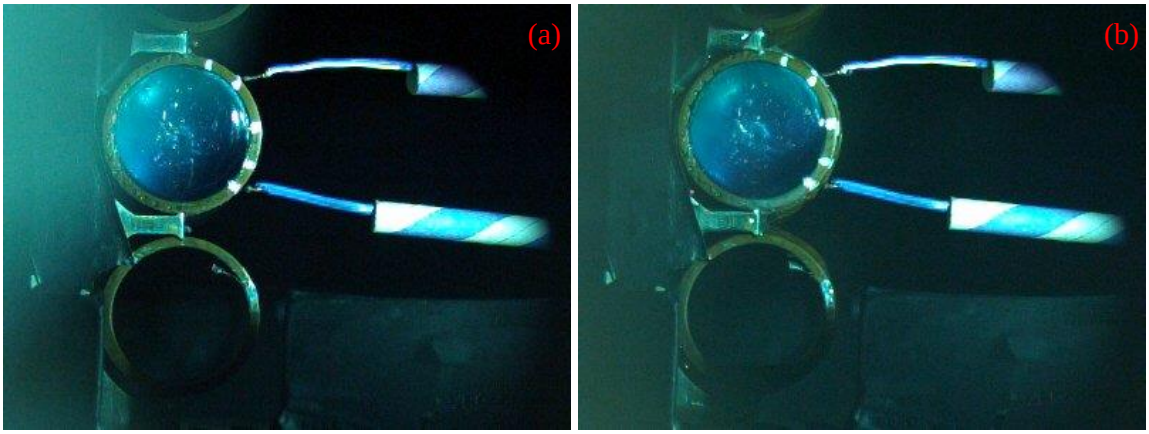

Fig. 4: Raw image of high speed camera (a) without flow and (b) with flow.

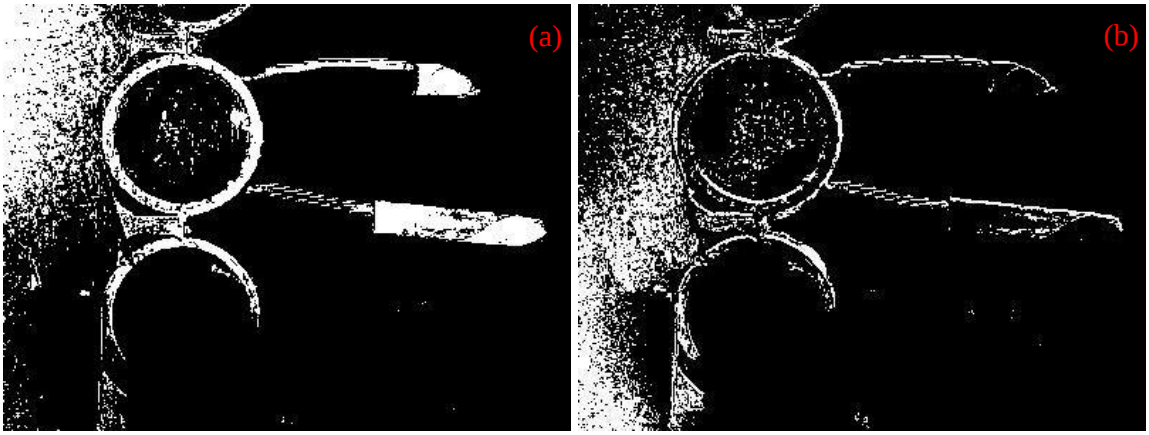

Fig. 5: Processed image of high speed camera (a) without flow and (b) with flow.

An in house ImageJ macro program is developed to identify the circumferential angle and generate radial intensity profile for without flow and with flow processed images. Figures 6a and 6b show the radial intensity profile for without flow and with flow processed images respectively. The macro program is developed for each circumferential angle of the plain tube ranging from $10^{o} \leq \theta \leq 170^{o}$ to obtain film thickness data.

After acquiring film thickness, the selected frames of high speed camera and the corresponding frames in high speed infra-red camera are used for the post processing using FLIR software. ImageJ macro program and MATLAB program are developed to identify the circumferential angle and to obtain film temperature. Figure 7 shows the temperature gradient around plain tube using FLIR software.

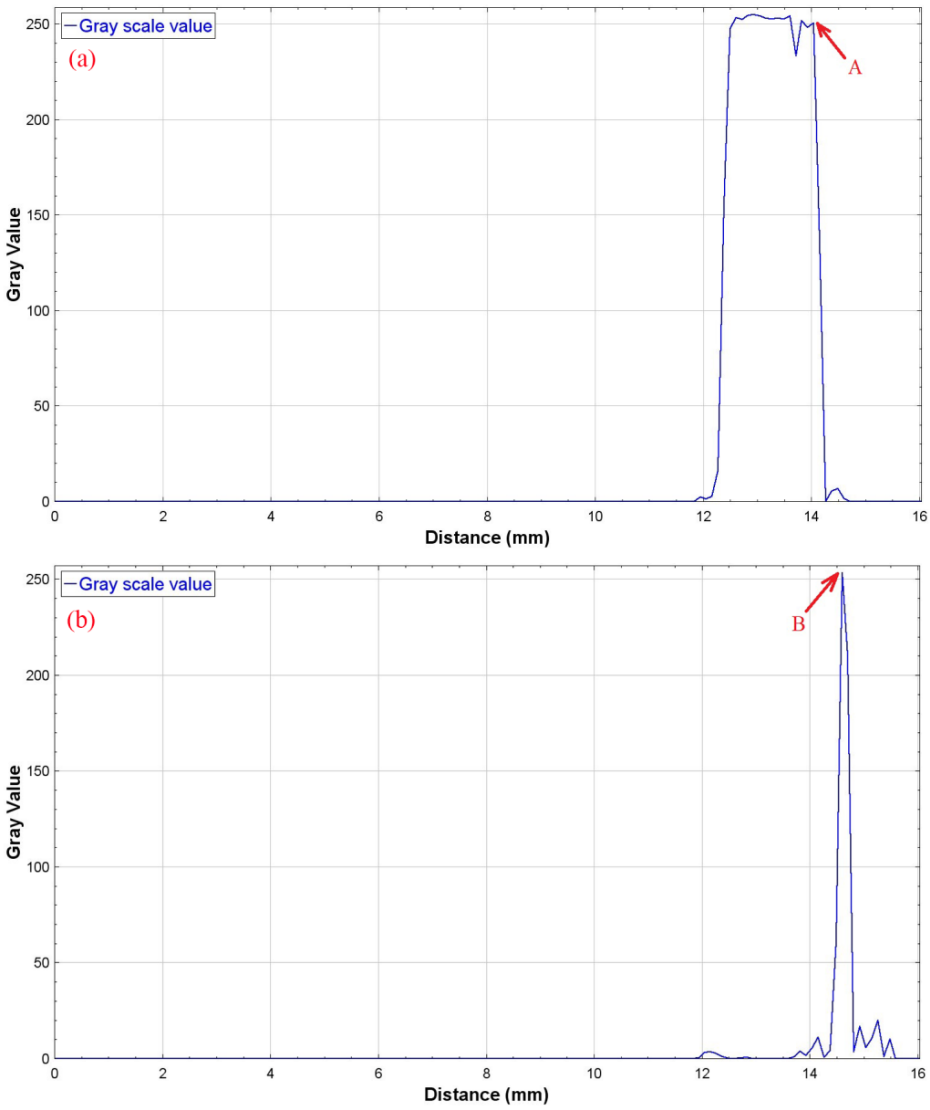

Fig. 6: Radial intensity profile for (a) without flow and (b) with flow of processed images at 80º circumferential angel.

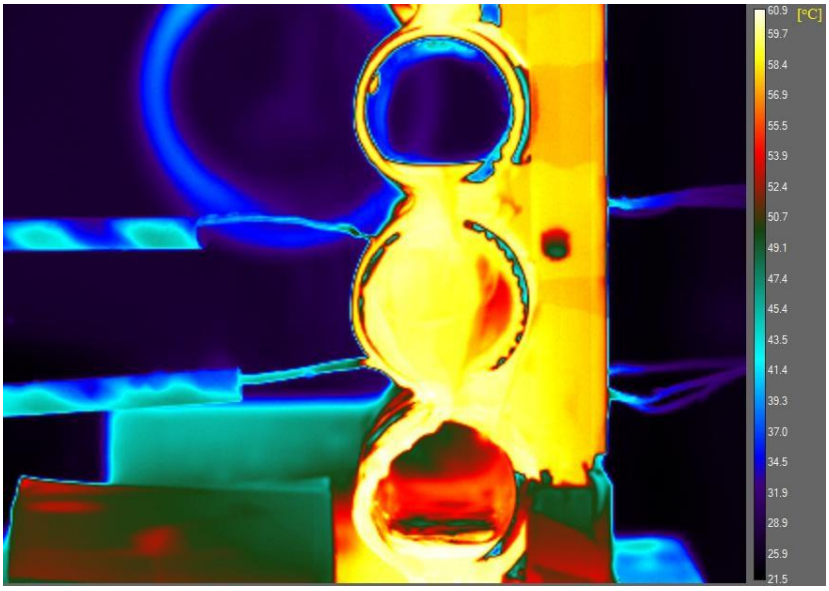

Fig. 7: Temperature gradient around plain tube using FILR software.

4. Empirical relations and Error analysis

4.1. Empirical relations

The falling film thickness (δ) over horizontal tube empirical Eq. 1 is given by Nusselt (Nusselt, 1916).

$$\delta = \left(\frac{3\mu_l \Gamma}{\rho_l(\rho_l - \rho_g) g \sin\theta}\right)^{1/3} \quad \text{(eq. 1)}$$

Where, μ_l – Liquid Dynamic viscosity [kg.m^{-1}.s^{-1}] ; Γ – Film flow rate per unit length on one side of the tube [kg.m^{-1}.s^{-1}] ; ρ_l – Liquid Density [kg.m^3] ; ρ_g – Vapor Density [kg.m^3] ; g – Acceleration due to gravity [m.s^{-2}] ; θ - Circumferential angle

In Nusselt's Eq. 1, falling film momentum effect was not taken into account. Therefore, Hou et al. has modified the Eq. 1 by considering diameter of the tube and impingement height, and the modified equation is given in Eq. 2.

$$\delta = C\left(\frac{3\mu_l \Gamma}{\rho_l(\rho_l - \rho_g) g \sin\theta}\right)^{1/3} \left(\frac{S}{D}\right)^n \quad \text{(eq. 2)}$$

Where, S – Impingement height [m] ; D – Tube diameter [m] ; n – Refractive index

$$C = \begin{cases} 0.97540, & 0^o < \theta \leq 90^o \\ 0.84978, & 90^o < \theta \leq 180^o \end{cases} \quad ; \quad n = \begin{cases} -0.16670, & 0^o < \theta \leq 90^o \\ -0.16479, & 90^o < \theta \leq 180^o \end{cases}$$

Reynolds number (Re) for falling film around the horizontal tube is given in Eq. 3.

$$Re = \frac{4\Gamma}{\mu_l} \quad \text{(eq. 3)}$$

4.2. Error analysis

A standard error mean analysis is carried out for all data sets for each circumferential angle (θ). Mean film thickness (δ_{mean}) and mean film temperature (T_{mean}) are computed by Eq. 4 and Eq. 5 respectively.

$$\delta_{mean} = \frac{\sum_{i=1}^{N} \delta_{i=1}}{N} \quad \text{(eq. 4)}$$

$$T_{mean} = \frac{\sum_{i=1}^{N} T_{i=1}}{N} \quad \text{(eq. 5)}$$

The standard deviation (SD) for the data sets is computed by Eq. 6.

$$SD = \sqrt{\frac{\sum_{i=1}^{N} (\delta_{mean} - \delta_i)^2}{N-1}} \quad \text{(eq. 6)}$$

The standard error mean (SEM) analysis is computed by Eq. 7.

$$SEM = \delta_{mean} \pm \frac{SD}{\sqrt{N}} \quad \text{(eq. 7)}$$

5. Results and discussion

Experimentation is carried out to determine the falling film thickness and temperature. The circumferential angle of falling film thickness and temperature are measured simultaneously, in the range $10^o \leq \theta \leq 170^o$ and $10^o \leq \theta \leq 180^o$, respectively, with an increment of 10^o.

5.1. Comparison with numerical correlation

Figure 8 shows the variation of falling film thickness around the circumference of the plain tube for the flow rate of 2 lpm, which corresponds to the Reynolds number of 1981.82. The momentum effect of liquid film from 80^o of plain tube circumferential angle is accounted as in Eq. 2. The surface tension force of liquid film plays an important role in the shift in minima from 90^o to 110^o circumferential angle of the plain tube. The film thickness at circumferential angels in the range of 0^o to 20^o and 160^o to 180^o of plain tube are higher and so, the liquid film has to slide over the vertical wall, reducing the momentum transfer. These regions are known as impingement zones and have the maximum error in the range of ±10.57% to ±12.27% for the film thickness. The average error

is in the range of ±1.77% to ±6.00% for the circumferential angles ranging from 30º to 150º. The present study for the circumferential angle at 80º with variation of Reynolds numbers for plain tube is compared with the experimental results carried out by Jayakumar and Mani, 2022 for plain tube with varying Reynolds numbers as shown in Fig. 9. The temperature of working fluid is maintained at 25ºC for Reynolds number ranging from 356 to 715, which corresponds to the flow rate of 0.72 lpm to 1.43 lpm. It is observed that the maximum error for the present study is in the range of ±3.2% to ±8.29%. The local heat transfer coefficient (h) with unit $W.m^{-2}.ºC^{-1}$ for different circumferential angles of plain tube is computed from Eq. 8 and plotted as shown in Fig. 10.

$$h = \frac{k_{eff}}{\delta_{mean}} \qquad \text{(eq. 8)}$$

Where, k_{eff} – effective thermal conductivity [m] ; δ_{mean} – Mean film thickness [m]

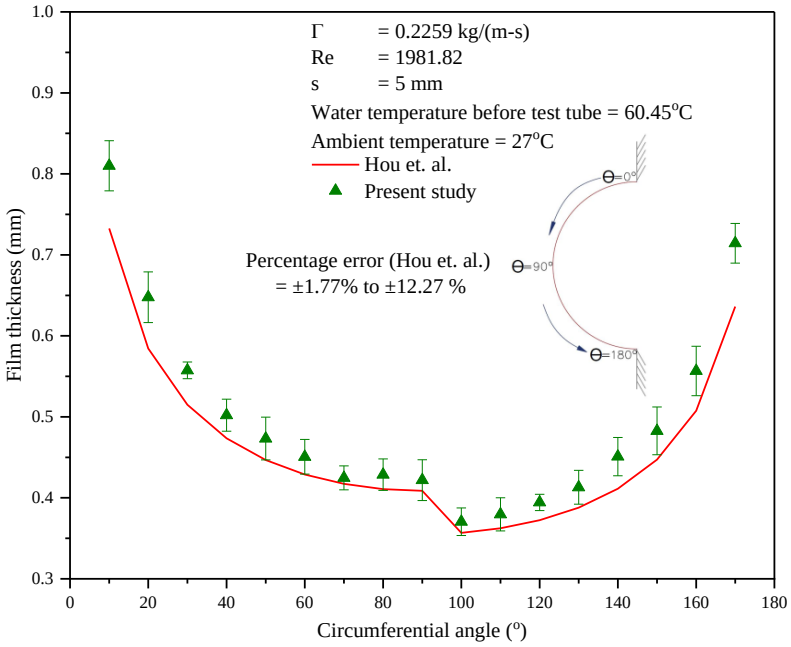

Fig. 8: Comparison of film thickness along circumferential angle with literature data.

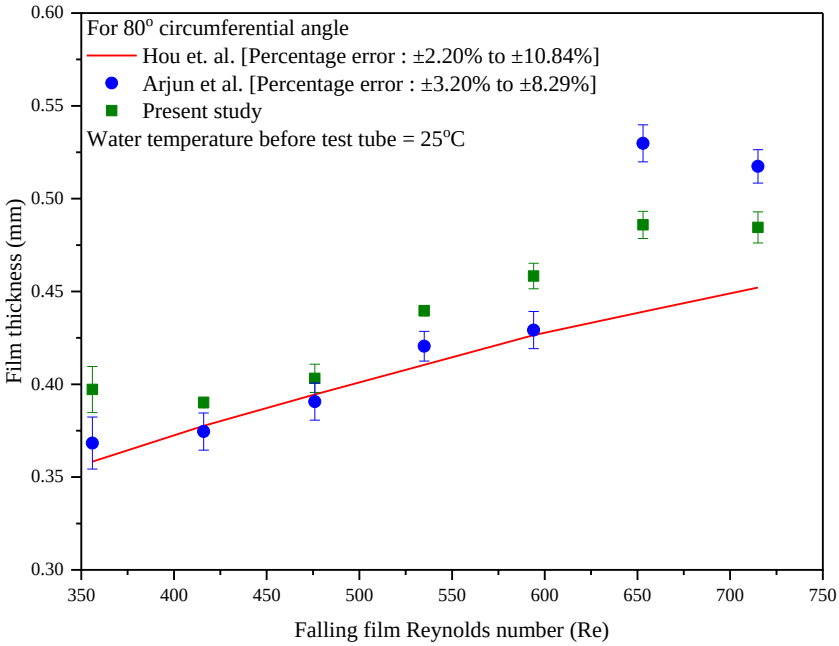

Fig. 9: Comparison of falling film thickness with different Reynolds numbers with literature data.

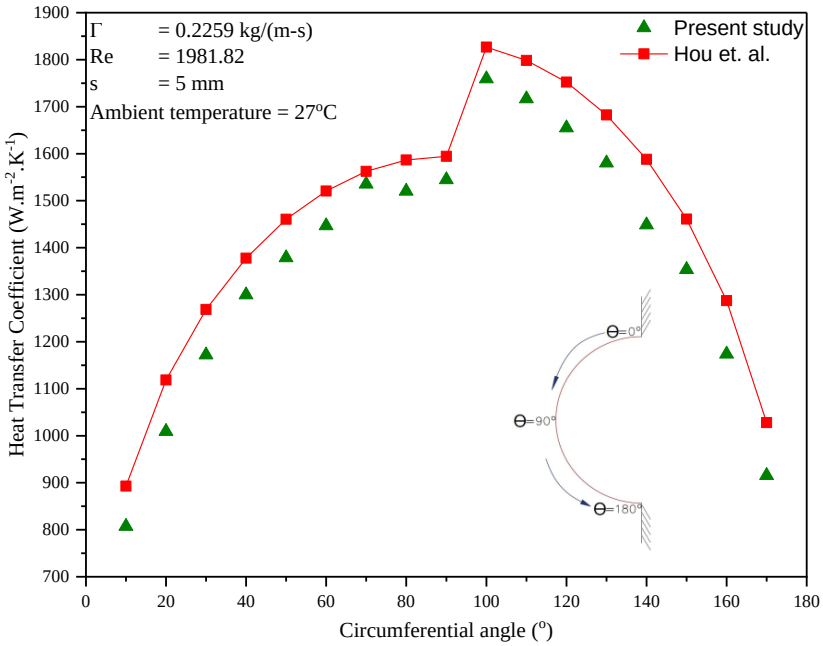

Fig. 10: Comparison of heat transfer coefficient along circumferential angle with literature data.

5.2. Effect of Reynolds number

Figure 11 shows the variation of falling film thickness around the circumference of the plain tube as a function of feed Reynolds number. The range of feed Reynolds number for typical MED operation is $448.213 \leq Re \leq 1981.82$. All the film thickness measurements are taken for complete wetting and taken as the effective length of plain tube and steady flow rate. It is observed that the falling film thickness variation around the circumferential angle of plain tube shows a strong correlation with Reynolds number variation.

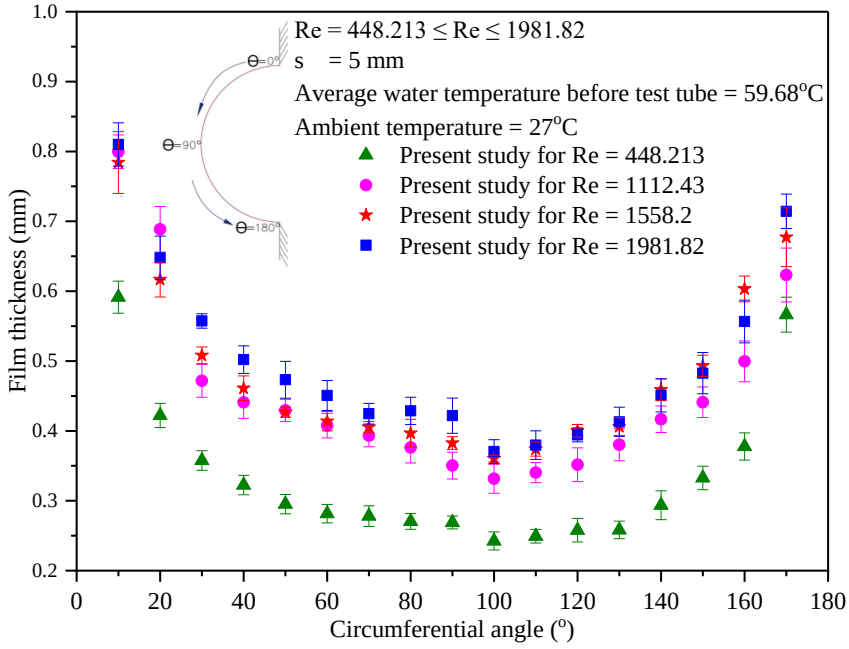

Fig. 11: Variation of falling film thickness with circumferential angle for different Reynolds numbers.

5.3. Effect of feed inlet temperature

Figure 12 shows the variation of falling film temperature around the circumference of the plain tube for the Reynolds number of 1981.82 which corresponds to 2 lpm. The average feed inlet temperature of test tube is 60°C.

All the temperature measurements are taken for complete wetting of the effective length of plain tube. The temperature data at 0º, 45º, 135º and 180º circumferential angles are measured using calibrated thermocouples. The error band of High Speed Infra-Red (HSIR) data is in the range of ±0.08% to ±1.57% when compared with calibrated T - type thermocouple. Figure 13 shows the variation of falling film temperature around the circumference of the plain tube as a function of feed Reynolds number.

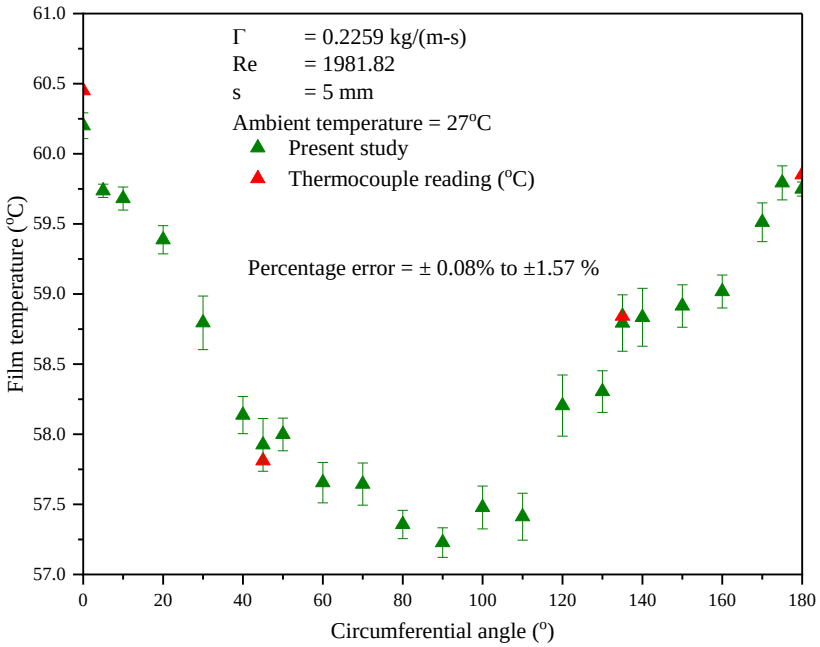

Fig. 12: Variation of falling film temperature with circumferential angle.

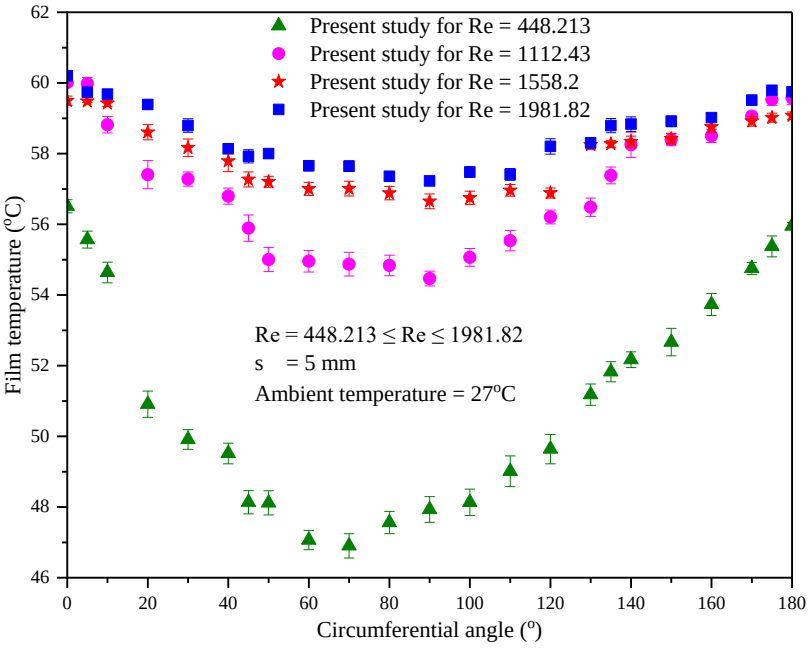

Fig. 13: Variation of falling film temperature with circumferential angle for different Reynolds numbers.

6. Conclusions

In this paper, an image processing technique (non - intrusive method) is used to evaluate the falling thin film thickness and film temperature around the circumference of a plain horizontal tube. This study is carried out for the circumferential angles ranging from 10º to 170º for film thickness and 0º to 180º for film temperature. The

film thickness follows the Hou et al., 2012 empirical model with the error band of ±1.77% to ±6.00% at non - impingement zones. Also, the present study of film thickness is compared with Jayakumar and Mani and has error band of ±3.20% to ±8.29% for different Reynolds numbers. The error band for falling film temperature is in the range of ±0.08% to ±1.57%, when compared with calibrated thermocouples.

7. References

Al-Shammiri, M., Safar, M., 1999. Multi-effect distillation plants: State of the art. Desalination 126, 45–59. https://doi.org/10.1016/S0011-9164(99)00154-X

Chen, X., Shen, S., Wang, Y., Chen, J., Zhang, J., 2015. Measurement on falling film thickness distribution around horizontal tube with laser-induced fluorescence technology. Int. J. Heat Mass Transf. 89, 707–713. https://doi.org/10.1016/j.ijheatmasstransfer.2015.05.016

Hou, H., Bi, Q., Ma, H., Wu, G., 2012. Distribution characteristics of falling film thickness around a horizontal tube. Desalination 285, 393–398. https://doi.org/10.1016/j.desal.2011.10.020

Jayakumar, A., Balachandran, A., Mani, A., Balasubramaniam, K., 2019. Falling film thickness measurement using air-coupled ultrasonic transducer. Exp. Therm. Fluid Sci. 109, 109906. https://doi.org/10.1016/j.expthermflusci.2019.109906

Jayakumar, A., Mani, A., 2022. Experimental and Numerical Study of Hydrodynamic and Heat Transfer Characteristics of Falling Film over Metal Foam Layered Horizontal Tube. J. Heat Transfer 144, 1–11. https://doi.org/10.1115/1.4053203

Khawaji, A.D., Kutubkhanah, I.K., Wie, J.M., 2008. Advances in seawater desalination technologies. Desalination 221, 47–69. https://doi.org/10.1016/j.desal.2007.01.067

Maliackal, A.K., Ganesan, A.R., Mani, A., 2022a. Heat transfer enhanced surfaces for horizontal tube falling film evaporator characterized using laser interferometry. Appl. Therm. Eng. 210, 118303. https://doi.org/10.1016/j.applthermaleng.2022.118303

Maliackal, A.K., Ganesan, A.R., Mani, A., 2022b. A novel interferometric method for simultaneous measurement of film thickness and film interface temperature for a horizontal tube falling film evaporator for MED systems. Int. J. Heat Mass Transf. 183, 122231. https://doi.org/10.1016/j.ijheatmasstransfer.2021.122231

Maliackal, A.K., Ganesan, A.R., Mani, A., 2021. Interferometric analysis of flow around a horizontal tube falling film evaporator for MED systems. Int. J. Therm. Sci. 161, 106745. https://doi.org/10.1016/j.ijthermalsci.2020.106745

Nair, M., Kumar, D., 2013. Water desalination and challenges: The Middle East perspective: A review. Desalin. Water Treat. 51, 2030–2040. https://doi.org/10.1080/19443994.2013.734483

Nusselt, W., 1916. Die oberflachenkondensation des wasserdamphes. VDI-Zs 30, 541.

Ophir, A., Lokiec, F., 2005. Advanced MED process for most economical sea water desalination. Desalination 182, 187–198. https://doi.org/10.1016/j.desal.2005.02.026

Xu, L., Ge, M., Wang, S., Wang, Y., 2004. Heat-transfer film coefficients of falling film horizontal tube evaporators. Desalination 166, 223–230. https://doi.org/10.1016/j.desal.2004.06.077

Zhang, Y., Wang, D., Liu, Y., Tang, M., Zhang, S., 2020. Distribution characteristics of falling film thickness around a horizontal corrugated tube. Int. J. Heat Mass Transf. 154. https://doi.org/10.1016/j.ijheatmasstransfer.2020.119773